ELSEVIER

Journal of Alloys and Compounds 310 (2000) 233–242

Journal of ALLOYS AND COMPOUNDS

www.elsevier.com/locate/jallcom

High precision measurement of torsion fiber internal friction at cryogenic temperatures

M.K. Bantel, R.D. Newman*

Department of Physics and Astronomy, University of California at Irvine, Irvine, CA 92697-4575, USA

Abstract

Cryogenic torsion pendulums being developed for research in gravitational physics serve well for exceptionally accurate measurements of nonlinear and anelastic properties of torsion fibers at low temperature (77 K and 4.2 K) at low frequency (~0.01 Hz) in a pre-plastic regime of high shear strain (0.0001–0.003). The measurements use a torsion pendulum suspended by a thin fiber (typically ~20 μm×24 cm), oscillating with an amplitude of many revolutions. In a few oscillation cycles, oscillation amplitude and frequency may be determined to better than one part in 10^8, and harmonic deviations from simple harmonic motion (at 77 K) with fractional accuracy better than 10^{-9}, enabling very accurate determination of the decrement, modulus defect, and hysteresis loop of the system as a function of oscillation amplitude.

Keywords: Torsion fiber friction; Cryogenic temperatures; Precision measurement

1. Introduction

The motivation for the work reported here arises in the field of experimental gravitational physics. Internal friction is a limiting factor in the measurement of extremely small forces, due to the thermal noise force with spectral density $F^2(f) = 4k_B Tb(f)$ which necessarily drives a system characterized by a dissipative damping factor b. This noise force disturbs the suspended end mirrors in interferometers designed to detect gravity waves, as well as large resonant bars used for the same purpose, motivating many efforts to understand the frequency dependence of internal friction and to find materials with minimal dissipation.

The torsion pendulum is an excellent instrument for precision tests of the Newtonian classical law of gravity, where the measurement of slowly modulated extremely weak forces is required. Such tests include searches for composition-dependence in the force between test masses, searches for deviation from inverse square distance dependence of the force, and measurement of the gravitational constant G. As the design of torsion pendulums has been progressively refined, thermal noise has become a limiting factor in their performance. This has motivated us to develop cryogenic torsion pendulums for gravity research, and to search for optimum torsion fiber materials. The torsion pendulum has an illustrious history [1] in the study of internal friction in materials, so it is not surprising that cryogenic pendulums, optimized for extremely sensitive measurements, serve well for studying the same material properties that limit them.

2. Internal friction and the measurement of the gravitational constant *G*

Our first step was to measure Q^{-1} as a function of oscillation amplitude for low frequency torsion pendulums with several candidate fiber materials: tungsten, copper beryllium, sapphire, and aluminum 5056. The results (Fig. 1) suggest that aluminum 5056 is a good choice for minimizing thermal noise. Sapphire gave better performance at small amplitude, but was unavailable in the small diameters needed for our work, and had the disadvantage of not providing a conducting path without a Q-degrading metallic coating. A striking feature noted in our data is the linearity of the amplitude dependence of Q^{-1} for the three metal fiber materials.

While we have a number of gravitational physics applications in mind for the instrument we are developing, our first goal is a measurement of Newton's gravitational constant G – motivated by large discrepancies among recent measurements of that least well known of the fundamental constants of nature. Our planned approach to

*Corresponding author.

E-mail address: rdnewman@uci.edu (R.D. Newman).

0925-8388/00/$ – see front matter
PII: S0925-8388(00)01010-0

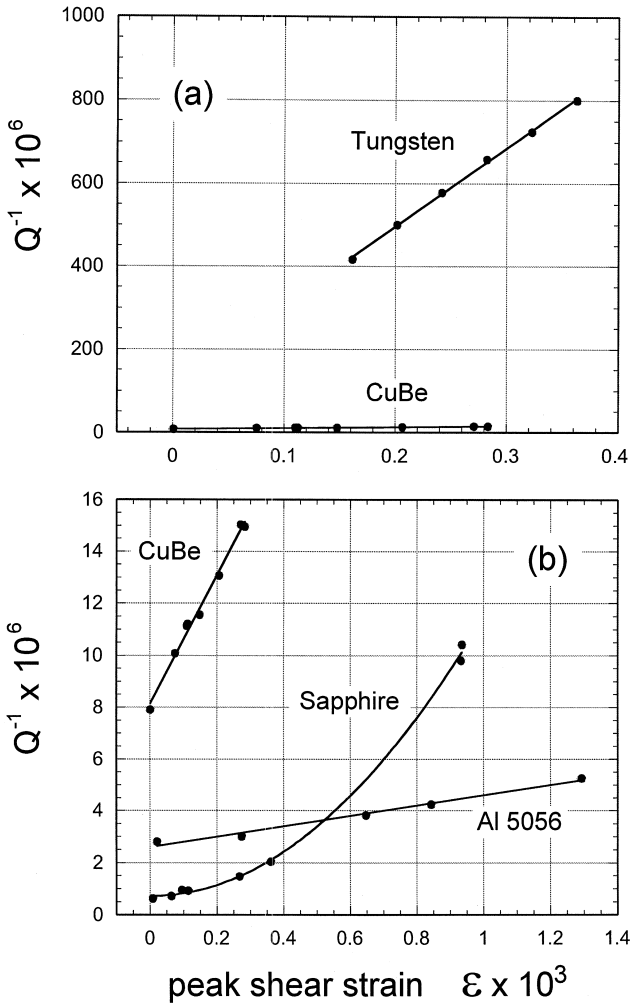

Fig. 1. Our early measurements of Q^{-1} at 4.2 K for several candidate torsion fiber materials, plotted against peak shear strain amplitude equal to the oscillation amplitude in radians times the ratio of fiber radius to length.

this measurement is a variant, with several novel twists [2], of the so-called 'dynamic' or 'time-of-swing' method. In this method, used in most of this century's measurements of G until recently, a pendulum suspended by a thin fiber undergoes torsional oscillation in the gravitational field of source masses. Oscillation frequencies are compared for two different positions of the source masses. The difference $\Delta\omega^2$ of the squares of the two measured frequencies is proportional to the gravitational constant: $\Delta\omega^2 = cG$, where the proportionality factor c is a known function of the mass distributions of the pendulum and source masses, and also a function of the pendulum's oscillation amplitude, but (for an ideal fiber) requires no knowledge of the fiber's torsion constant. The method has great advantages: it is based on a measurement of frequency which can be made very accurately, it requires no precision measurement of angular displacement, and it apparently requires no calibration of the fiber torsion constant. Alas, the method has a peril arising from the fiber's internal friction, which was recently pointed out by the Japanese physicist Kazuaki Kuroda [3].

The apparent absence of dependence on fiber torsion constant in the relation $\Delta\omega^2 = cG$ rests on an assumption that the effective mechanical torsion constant is the same for both positions of the source masses. But because of anelastic effects in the fiber, this will not be the case. In fact, the measured frequency difference will be related to G by: $\Delta\omega^2 = cG + [k(\omega_1) - k(\omega_2)]/I$ where I is the pendulum's moment of inertia and $k(\omega_1)$ and $k(w_2)$ are the effective torsion constants at the oscillation frequencies corresponding to the two mass positions. If the term with $k(\omega)$ is neglected, the inferred value of G will be too high. Experimental evidence of this effect has been subsequently found [4].

Kuroda showed that if fiber internal friction is characterized by a complex frequency-dependent torsion constant with a ratio of real to imaginary parts which is frequency independent, as is found experimentally to be approximately the case for many materials over a considerable range of frequencies [5,6], then the resulting bias error in G will be given by $\delta G/G = Q^{-1}/\pi$ where Q is the quality factor of the pendulum. If one could be confident of this assumed fiber character, the G correction would be calculable and in any case very small for an instrument with a Q on the order of 3×10^5 such as would be achieved with an aluminum fiber at 4.2 K. In fact, we have shown [2] that even if the ratio of imaginary to real parts of k is an unknown function of frequency, still, as long as the anelasticity is *linear*, characterized by a continuum of Maxwell units [7] with an arbitrary strength or frequency distribution, then the resulting bias in G will be bounded: $0 \leq \delta G/G \leq \frac{1}{2}Q^{-1} + O[Q^{-2}]$. In that case the G bias, although uncertain in exact magnitude, would still be too small to be a limitation in forseeable G measurements.

But another concern must be addressed. Kuroda's expression for $\delta G/G$ and our generalization of it both assume linear anelasticity. Linearity implies that Q may depend on frequency but not on amplitude, while in fact Fig. 1 displays a significant amplitude dependence (and hence nonlinearity) of internal friction in all fibers tested. What can be said about the frequency dependence of the torsion constant arising from this nonlinear component of internal friction? In principle, one could measure $k(\omega)$ directly with a sequence of pendulums with different moments of inertia but the same mass to assure constant loading – such measurements have been made by Kuroda and his associates [8]. However, in order to measure G with a given fractional accuracy, such a fiber study must be made with moments of inertia measured with an equal fractional accuracy. To do this to 1 ppm, as would be desired, is practically out of question.

Recently reported G measurements and those currently under way or planned, mindful of possible fiber problems, have avoided use of the 'dynamic' method. However, the several advantages of that method are so attractive that we

have chosen to attempt to understand fiber behavior sufficiently well that we can confidently bound possible bias from anelasticity. This has led us into a fascinating field, with interesting results.

3. The fiber study method

3.1. The fiber, pendulum, and damping system

Although A1 5056 is the fiber material we expect to use most in our gravitation experiments, our initial study reported here is of a CuBe fiber because of the larger nonlinear damping it exhibits. The CuBe fiber is alloy 25, COA 172 (~2% Be). It was tested as received from its manufacturer, California Fine Wire, where it was hard drawn with an approximate 11% area reduction between dies. The tested fiber has diameter 20 μm, effective length 24 cm, and a torsion constant ~0.03 dyn-cm/rad. At its ends it is glued with Stycast 1266 epoxy into small aluminum tubes mounted with screws to the suspension point and to the pendulum.

The pendulum body is an aluminum disk with a vertical aluminum shaft on which four symmetrically oriented vertical mirror surfaces are diamond machined. As the pendulum rotates a mirror surface faces an optical readout axis every 90 degrees of rotation. The pendulum has mass 11.2 grams and moment of inertia 20.5 g cm^2, which with the CuBe fiber gives an oscillation period of about 160 s. The pendulum loads the fiber to about 30% of its yield strength.

The pendulum operates in a framework (Fig. 2) within a vacuum chamber surrounded by liquid nitrogen or helium. An important feature is a damping system for swinging motion of the pendulum: the CuBe fiber is coupled at its upper point to an aluminum damping disk suspended between the poles of a pair of ring magnets with iron return path. This disk is in turn suspended from a rigid upper mount by an 8 cm 380 μm diameter phosphor bronze wire. Swinging motion of the pendulum induced by ambient microseismic motion is transferred to transverse motion of the disk, where induced eddy currents serve to absorb the energy of this mode. This system reduces the *Q* of the pendulum's swinging mode from a very high value to about 52 at room temperature. Both because the upper thick fiber is torsionally very stiff, and because of the azimuthal symmetry of the magnetic field, the dissipation of energy in the pendulum's torsional mode by this damping system is completely negligible.

A stepper motor allows adjustment of the equilibrium angular position of the pendulum, and may also be used to draw up the 'elevator plate' shown in the diagram. This presses the pendulum against a copper plate on the cold frame, protecting the pendulum during initial installation and final removal of the system, and cooling it during system cooldown. Vacuum in the system is maintained by an 8 l/s ion pump and improved by a charcoal cryopump within the vacuum chamber.

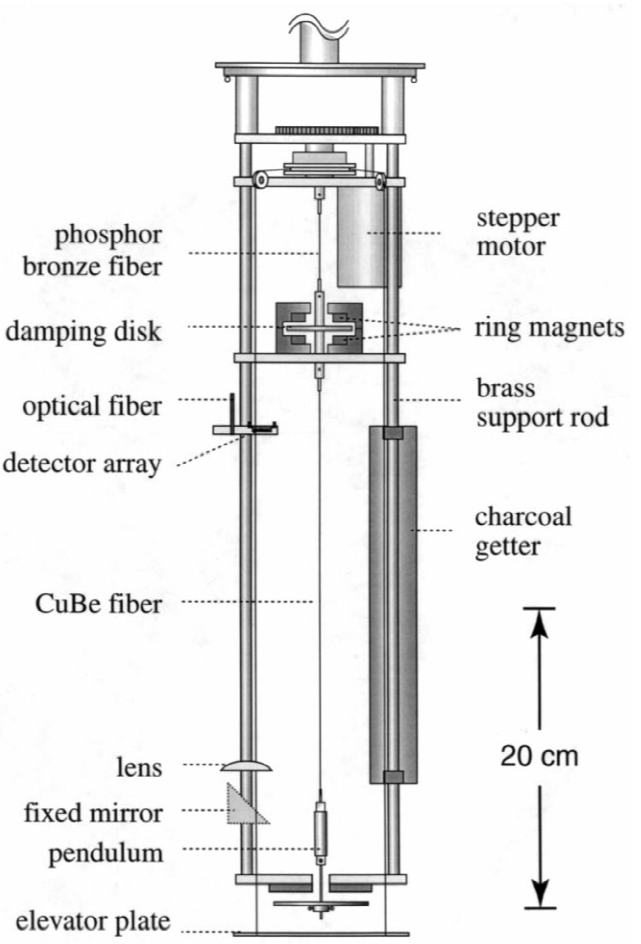

Fig. 2. Scale drawing of the pendulum system used for fiber tests, showing the optical readout system, cryopump, elevator plate used to support the pendulum during installation and cooldown, and the double pendulum with damping disk used to damp pendulum swinging motion.

3.2. Optical readout system

A folded path autocollimator system views the mirror faces of the pendulum (Fig. 3). Light from a 2.5 mW (max) 820 nm LED at room temperature is brought by a 100 μm optical fiber to the focal plane of a 200 mm focal length lens. The lens columnates the light, which is then directed toward the pendulum by a 45 degree mirror. From a pendulum's mirror face the light may return by nearly the same path to a focal point which sweeps across the 0.9 mm×4.0 mm elements of a Centronics LD2O-5 20 element PIN photodiode array in the lens focal plane. Alternate elements of this array are wired together and input to a differential amplifier, generating a 'transit' signal as indicated in Fig. 3. In addition to this 'normal' path, there is a 'side' path in which light is imaged on the array after reflection from the pendulum to a mirror fixed on the instrument framework, back to the pendulum, and

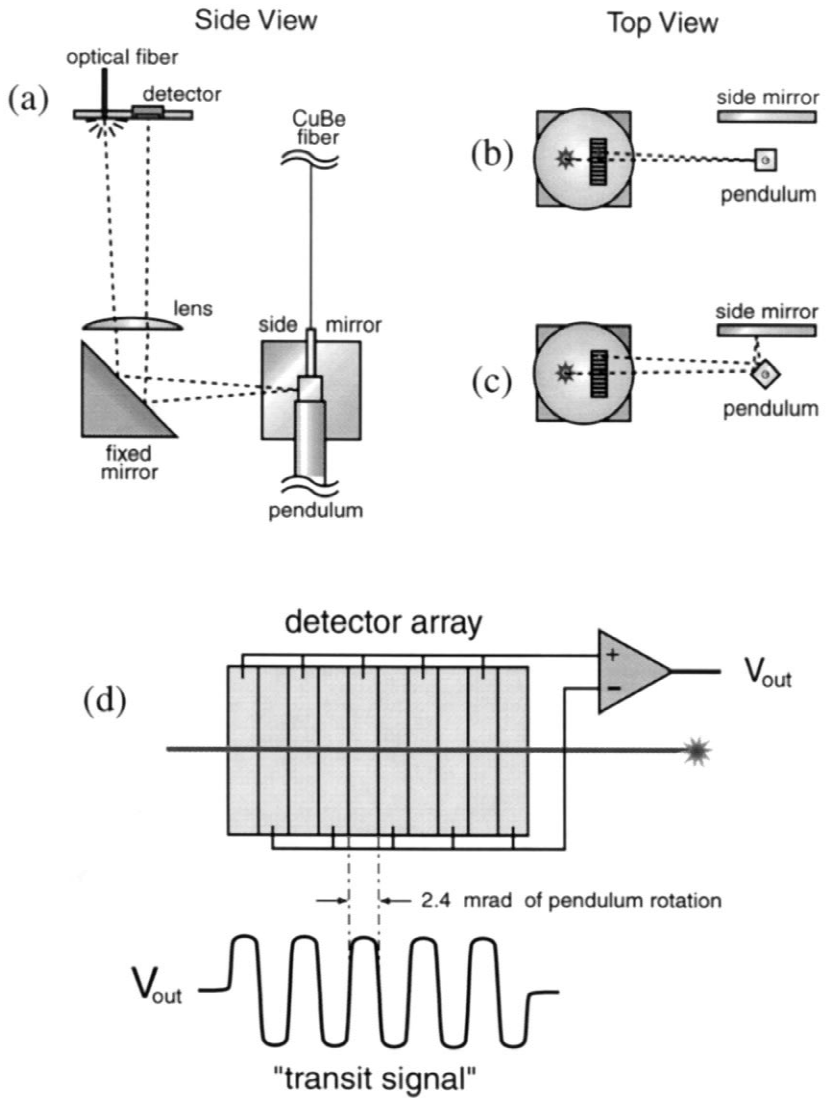

Fig. 3. (a) Schematic drawing of the optical readout system, side view. (b) Top view, indicating the light source and multi-element detector in the lens focal plane and the 'normal' light path which produces transit signals at $\theta = 0°$, 90°, 180°, and 270°. (c) The 'side' light path, which produces transit signals at $\theta = 45°$, 135°, 225°, and 315°. (d) path of the 100 μm imaged light spot across a portion of the multi-element detector, and the resulting output voltage signal, one of whose zero crossings defines the transit instant.

then to the lens focal plane. This side path generates a transit signal when one of the mirror faces makes an angle of 45 degrees with the optical axis. Thus in each revolution of the pendulum the two paths generate a total of eight transit signals, corresponding to pendulum orientations at 45 degree intervals.

The transit signals are digitized at 50 ks/s with a 16 bit ADC in a PC computer. A third degree polynomial fit is made to the sampled voltages as a function of time in the region of the signal zero crossings; the zero crossing of this fitted polynomial measures the instant at which the pendulum had a particular orientation.

3.3. Data processing

For an amplitude of N revolutions (a total of $4N$ pendulum rotations per cycle), the readout yields $32N$ time points per cycle, corresponding to relative angular orientations which are known exactly for transits an integral number of revolutions apart, and determined for all other transit pairs by a total set of seven unknown parameters δ_m which reflect uncertainty in the relative orientations of the pendulum's four mirror faces and of the fixed side mirror. Data were taken with pendulum oscillation amplitudes as much as 80 radians, yielding up to 400 time data points per oscillation cycle, each determined with accuracy of about one microsecond. These times and corresponding angles, $\{\theta_i, t_i\}$, are fitted to a function:

$$\theta(t) = c_0 + c_1 t + e^{-\gamma t} \sum_{n=1}^{7} [A_n \cos(n\omega t) + B_n \sin(n\omega t)] \quad (1)$$

where the fitted parameters include c_0, c_1, γ, ω, the

harmonic coefficients, and also the seven free parameters which fix the unknown relative mirror orientations. The parameter c_0 represents an offset of the pendulum's equilibrium position relative to the mirrors, while c_1 represents a linear drift of this position with time over the duration of the fitted region. Fits are normally made to data sets corresponding to only two cycles, since the frequency ω, damping factor γ, and relative harmonic coefficients A_n and B_n are all functions of oscillation amplitude. The fits are significantly improved by introducing two new free parameters to represent a linear time dependence of ω and γ within the two cycle fit. In fitting each oscillation segment, the time origin is chosen so that the fitted coefficient A_1 is zero so that the relative values of the other harmonic coefficients may be compared consistently over the course of a long data run. The fitted values of the mirror position parameters were consistent to a fraction of a microradian over wide ranges of oscillation amplitude, giving confidence that the determination of harmonic amplitudes is not distorted by error in mirror position determination.

3.4. Determination of amplitude dependent fiber properties

The fits described above determine the frequency $\omega(A)$ and damping $Q^{-1}(A)$ with extraordinary accuracy. The pendulum's oscillation period and amplitude may be determined to about one part in 10^8 in one oscillation cycle, while a Q of 10^4 or more may be determined to a few parts in 10^4 from the oscillation decay over only four cycles. The accurate measurement of θ at a large set of time points effectively measures the function $\theta(t)$ describing the pendulum's oscillation – this in turn determines the torque $\tau(t) = I\ddot{\theta}$ that the fiber exerts on the pendulum. Knowing $\theta(t)$ and $\tau(t)$ one may then plot the hysteresis curve for the oscillation. One may use $\tau(t)$ to attempt to learn the functional dependence of τ on a set of variables characterizing the pendulum's motion: A, ω, θ, and $\dot{\theta}$.

In the rest of this paper we switch notation: θ will be written as x, $\dot{\theta}$ as $\dot{x}$ or v, and torque as F, emphasizing the analogy with a linear spring system. Thus our question becomes: given $x(t)$ and hence $\ddot{x}(t)$ and $F(t)$, what is the functional form of f in the following equation:

$$-m\ddot{x} = F = kx + k_2x^2 + k_3x^3 + f(A,\omega,x,\dot{x}) \quad (2)$$

4. Sample results

In the following discussion, strain amplitudes are discussed in terms of pendulum oscillation amplitude expressed in radians. The shear strain amplitude within the fiber at a given oscillation amplitude is proportional to radius, reaching a value of about 0.001 at an oscillation amplitude of 25 radians. Data were taken at amplitudes up to 70 radians, where the peak shear stress is about 15% of the yield strength of CuBe at 77 K. The fiber would have broken if twisted by about 600 radians. The pendulum loaded the fiber with a tension stress of 3.5×10^8 N/m^2, about 30% of the yield strength. Thus both the shear strain and tension loading in the regions explored are a significant fraction of yield strengths.

4.1. $Q^{-1}(A)$ at 77 K

Fig. 4a displays Q^{-1} as a function of amplitude during a six day segment of one data run during which the oscillation amplitude of the undisturbed pendulum decayed. For this run, Q^{-1} was determined for four-cycle data segments; each data point in the figure represents the average of Q^{-1} for 50 such consecutive segments. The extreme linearity of the amplitude dependence is remarkable. In fact, the small residuals from a linear fit to to this data (Fig. 4b) can be largely attributed to ambient temperature variation – the plot of measured temperature variation in the liquid nitrogen bath (dashed curve), when scaled and translated horizontally to account for time delay between the temperature variations of fiber and bath (solid curve), matches the observed Q^{-1} residuals quite exactly. This suggests that if the temperature of the system had been perfectly constant, the deviation of Q^{-1} from a linear fit would have been at most about a part in 10^4 of the total variation in Q^{-1} during the run. However, above about 70 radians and below 2 radians the data (not shown) deviate significantly from linear A dependence.

4.2. $Q^{-1}(A)$ vs. T

Fig. 5 indicates that the slope of $Q^{-1}(A)$ is nearly the same at 77 K and 4.2 K, although the zero amplitude limit at 4.2 K is a factor of about 3.5 smaller. This suggests that the CuBe fiber's internal friction has two independent contributions: $Q^{-1} = Q_{\mathrm{I}}^{-1}(T) + Q_{\mathrm{II}}^{-1}(A)$, where Q^{-1} is temperature dependent but amplitude independent and arises from a linear mechanism, while Q_{II}^{-1} is amplitude dependent but temperature independent. One must question whether the observed amplitude dependence arises in the fiber itself, or might arise in internal friction in the epoxy used to mount the fiber at its ends. To answer this question, we placed four drops of the same epoxy along the length of the fiber near its top, forming blobs surrounding the fiber with radius large compared to that of the fiber. This should amplify the effect of the glued fiber mounts by a factor of 5. In fact, plot c in the figure indicates that although the glue drops significantly changed the zero amplitude limit of Q^{-1},the slope changed by at most a few percent. We conclude that the observed amplitude dependence of Q^{-1} indeed arises in the fiber and is not associated with the epoxy glue mounts.

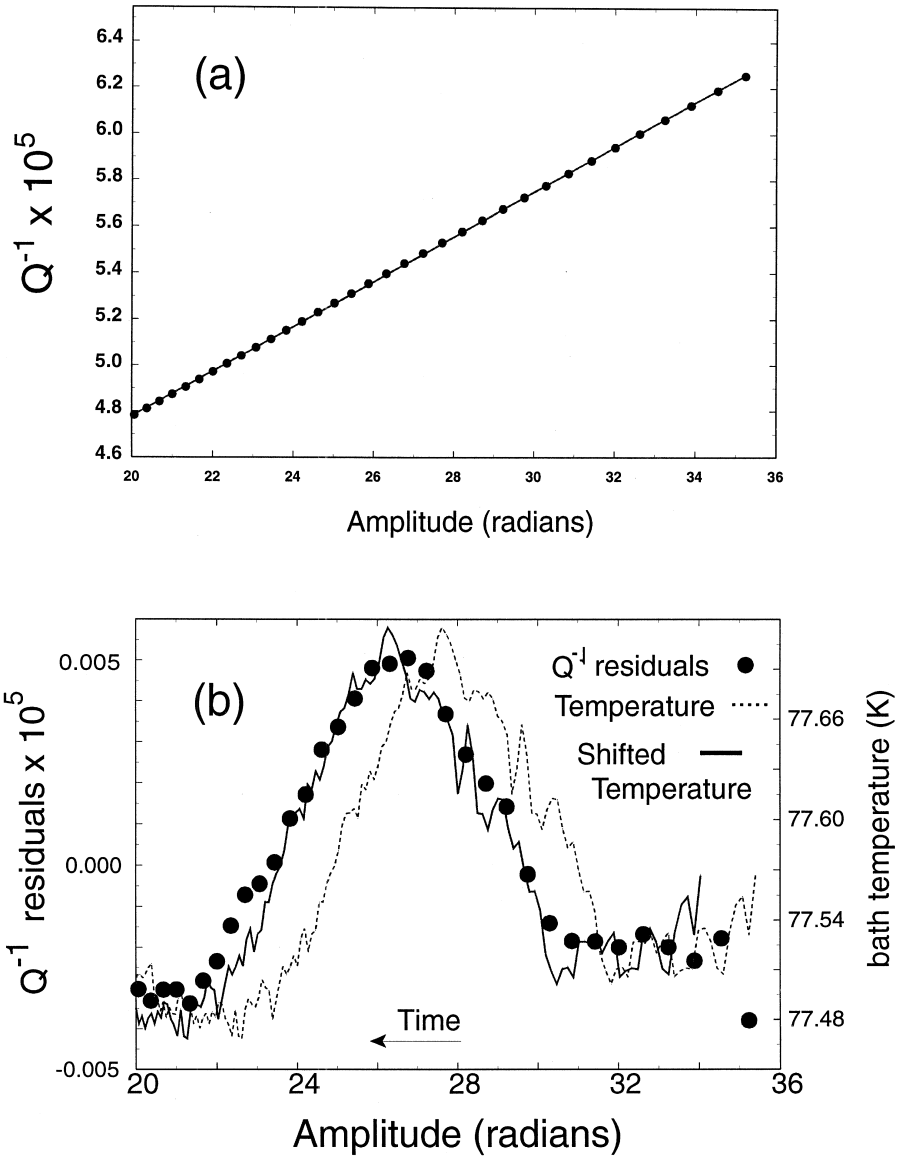

Fig. 4. (a) Q^{-1} vs. oscillation amplitude for the CuBe fiber during a six day segment of a run at 77 K, with a linear fit (solid line). Time runs to the left in the plot. (b) Solid circles: Residuals of the linear fit in plot a (scale to left, compare with scale in plot a). Dashed line: Temperature of the liquid nitrogen bath at corresponding times during the run (scale to right). Solid line: Temperature plot translated horizontally to overlay Q residual plot; the close match suggesting that the small residuals in plot 'a' are predominantly due to temperature variation, not amplitude variation.

4.3. The elastic force term k_2x^2

A term k_2x^2 in Eq. (2) leads to motion given to first order in k_2/k by:

$$x(t) = A\sin(\omega t) - \frac{1}{2}\frac{k_2}{k}A^2 - \frac{1}{6}\frac{k_2}{k}A^2\cos(2\omega t) \qquad (3)$$

implying an amplitude-dependent central position offset x_0 and harmonic amplitude A_2 (Eq. (1)) given by:

$$x_0 = -\frac{1}{2}\frac{k_2}{k}A^2 \quad A_2 = -\frac{1}{6}\frac{k_2}{k}A^2 \qquad (4)$$

each proportional to A^2, with amplitude-independent ratio $x_0/A_2 = 3$. The fitted values of x_0 and A_2 for data at 77 K are plotted in Fig. 6, revealing precise agreement with a A^2 amplitude dependence. The inferred value of k_2/k at 77 K is $(3.534\pm0.001)\times10^{-7}$ rad^{-1}. The ratio of the fitted coefficients of A^2 for the two plots is 3.04 ± 0.01, agreeing to ~1% with the expected ratio of 3. The small difference from 3 in the measured ratio could be attributed to a continuous drift in the equilibrium angle of the fiber of about 0.8 μrad/day. The statistical uncertainty in each data point in the harmonic A_2 is about 20 μrad, based on the scatter (relative to a locally fitted curve) of A_2 values from individual four cycle fits. The typical uncertainty of one of the plotted points is shown in Fig. 6 magnified by a factor of 1000.

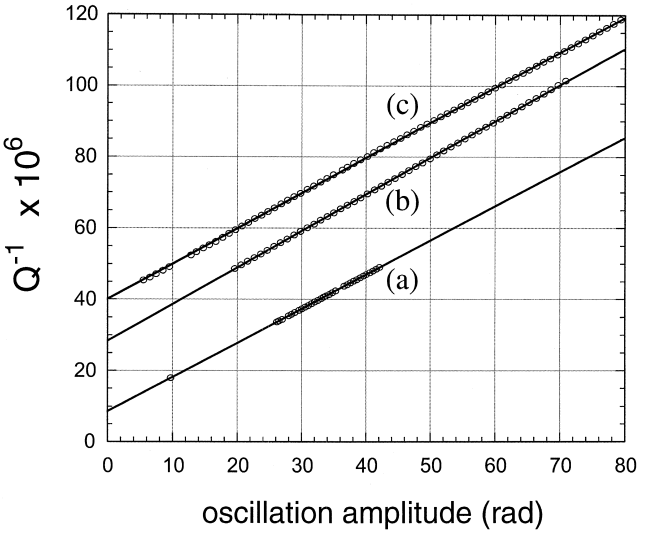

Fig. 5. Q^{-1} vs. oscillation amplitude for the CuBe fiber; solid lines are linear fits (a) at 4.2 K, (b) at 77 K, and (c) at 77 K after placing four epoxy drops along the fiber. This demonstrates that the variation of Q^{-1} with amplitude does not arise in the epoxy fiber mounts.

There is no reason to expect a non-zero value of k_2 in Eq. (2), given the apparent symmetry of the system, but our data clearly demonstrates its presence. This exercise gives us considerable confidence in our ability to measure harmonic coefficients.

4.4. The elastic force term k_3x^3

This force adds an additional harmonic $B_3 \sin(3\omega t)$ to Eq. (3), and also shifts the oscillation frequency. To first order in k_3/k we expect:

$$B_3 = -\frac{1}{32}\frac{k_3}{k}A^3 \quad \frac{\Delta\omega^2}{\omega_0^2} = \frac{3}{4}\frac{k_3}{k}A^2 \tag{5}$$

Fig. 7 displays the measured harmonic coefficient B_3, with an excellent single parameter fit to a cubic amplitude dependence which determines k_3/k at 77 K to be $(-4.860\pm0.003)\times10^{-8}$ rad^{-2}. Comparison of the predicted frequency shift with data will be made in Section 4.6 below.

4.5. Measurement of higher harmonics

Our analysis extracts the amplitude dependencies of harmonics up to seventh order with high precision; for example, Fig. 8 displays the coefficients B_6 and B_7 of the $\sin(6\omega t)$ and $\sin(7\omega t)$ harmonics at 77 K. One may note that the error bars on the plotted points are about 20 nanoradians, a few parts in 10^{10} of the oscillation amplitude.

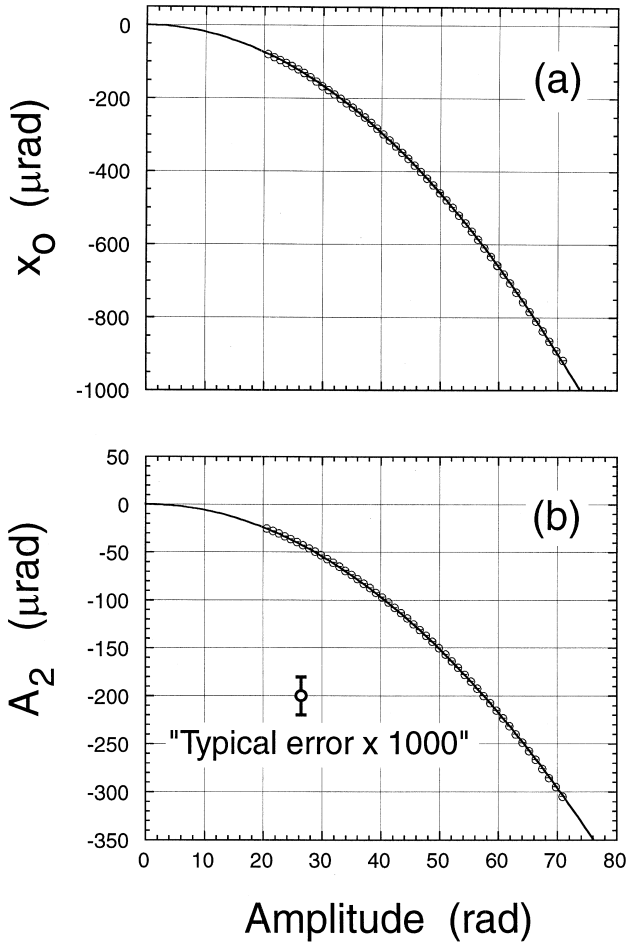

Fig. 6. Manifestations of an elastic k_2x^2 term in the CuBe fiber torsion constant at 77 K. (a) the central (mean) angular position x_0 as a function of oscillation amplitude, with a single parameter fit to a function c_aA^2. (b) the harmonic coefficient A_2 of $\cos(2c\omega t)$, with a single parameter fit to c_bA^2. The size of a typical statistical error bar for a data point is shown magnified by a factor of 1000.

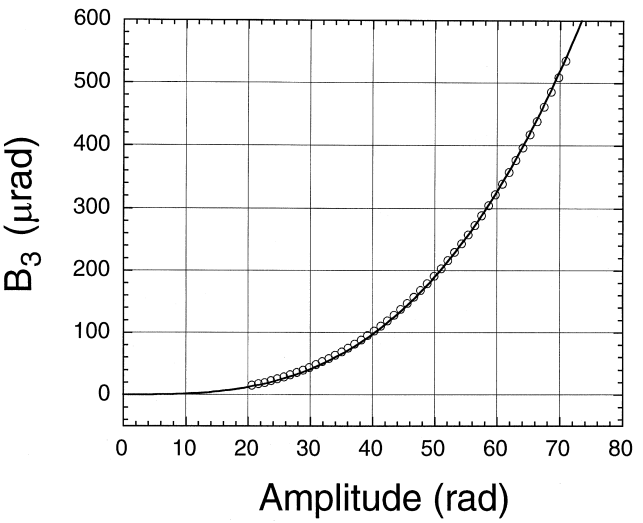

Fig. 7. Manifestation of an elastic k_3x^3 term: the harmonic coefficient B_3 of $\sin(3\omega t)$ at 77 K as a function of oscillation amplitude, with a single parameter fit to a function cA^3.

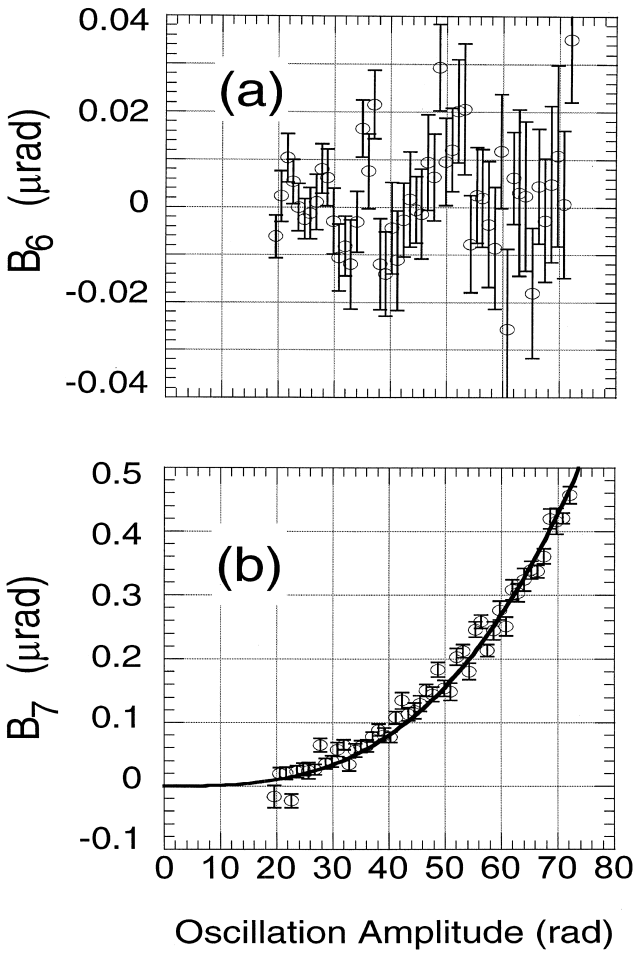

Fig. 8. Samples of measured higher oscillation harmonics as a function of oscillation amplitude: (a) the coefficient B_6 of sin(6ωt), (b) the coefficient B_7 of sin(7ωt). The statistical error bars are typically on the order of 20 nanoradians, to be compared with the oscillation amplitudes which are larger by a factor of more than 10^9.

4.6. Interpretation of the amplitude dependencies of Q^{-1} and $\Delta\omega^2$

A simple 'stick-slip' picture of friction predicts non-linear behavior close to what we observe. In this picture [9], a real spring is modeled as an ideal spring coupled to a string of blocks resting on a surface, connected by springs. Each block is statically bound to the surface until the net force on the block exceeds a certain threshold, at which point it breaks loose and moves freely until the net force drops below the threshold. The resultant effective force which must be added to the differential equation for a harmonic oscillator may be shown [10] to be of the form:

$$f[x, A, \hat{v}] = k_{ss}[(A^2 - x^2)\hat{v} - 2Ax] \quad (6)$$

where A is the oscillation amplitude and $\hat{v}$ is a unit vector in the direction of the velocity. This leads to a motion with a number of characteristic features, as discussed by Lebedev [11]:

(i) a linear variation of Q^{-1} with amplitude: $dQ^{-1}/dA = \text{constant}$
(ii) a linear variation of ω^2 with amplitude: $d\omega^2/dA = \text{constant}$
(iii) a specific ratio of the above variations: $r \equiv -\pi\omega_0^2 \Delta Q^{-1}/\Delta\omega^2 = 4/3$
(iv) a characteristic pointy 'Davidenkov' [11] hysteresis loop.

We now ask, how well do our results fit this picture?

(i) We have already seen that the variation of Q^{-1} with amplitude is strikingly linear at both 77 K and 4.2 K.

(ii) To test for a linear variation of ω^2 with amplitude, we must first subtract the contribution to $\Delta\omega^2(A)$ which arises from the k_3x^3 elastic force term (Eq. (5)), which we can do since we have determined k_3 with high precision from the harmonic amplitude B_3. The magnitude of this contribution is about one third of the total frequency shift at an amplitude of 40 radians. Fig. 9 displays the measured

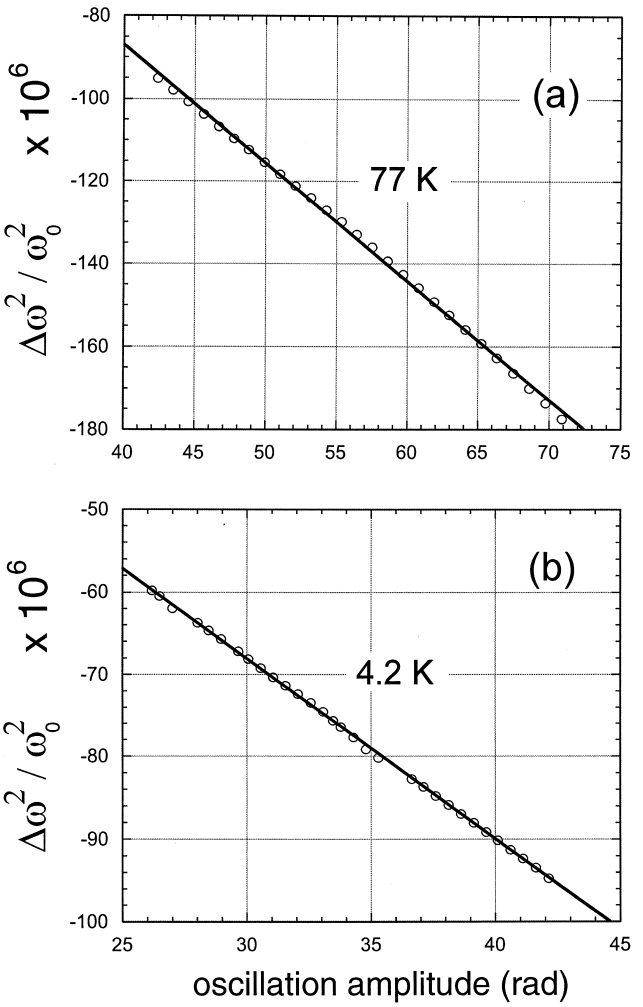

Fig. 9. The amplitude dependence of pendulum frequency for the CuBe fiber after subtracting the contribution expected from the k_3x^3 force term, using values for k_3 determined from the harmonic amplitude B_3, at (a) 77 K and (b) 4.2 K. The solid lines are linear fits.

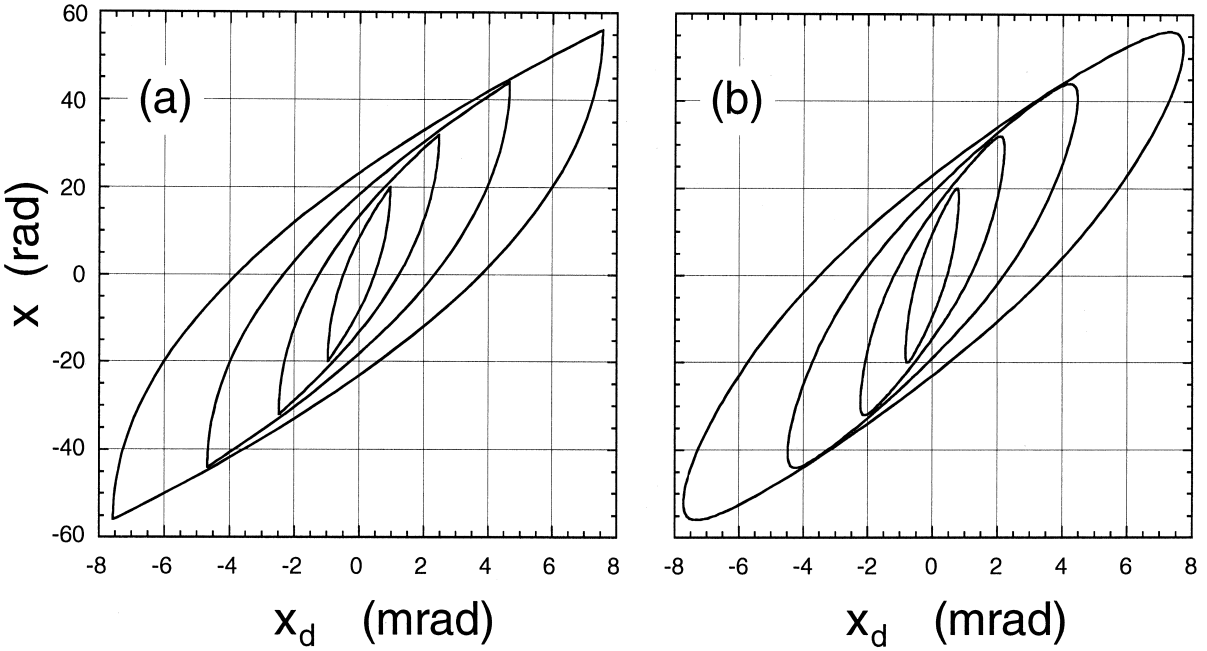

Fig. 10. (a) Hysteresis curves for a set of oscillation amplitudes of the CuBe fiber at 77 K which are implied by Eq. (6) using a value of k_{ss} determined from the measured slope dQ^{-1}/dA. (b) Corresponding experimentally determined curves, constructed from the measured harmonic amplitudes.

amplitude dependence of $\Delta\omega^2$ at 77 K and 4.2 K after making the subtraction; the residual amplitude dependence is indeed quite linear at both temperatures.

(iii) From the measured slopes dQ^{-1}/dA and $d\omega^2/dA$, at $T=77$ K we find the ratio to be $r=1.09\pm0.01$, while at $T=4.2$ K we find $r=1.31\pm0.01$, remarkably close to the ratio $r=1.33$ implied by the simple stick-slip model.

(iv) Fig. 10 shows the hysteresis loops expected from the force given by Eq. (6), and the corresponding measured hysteresis loops at 77 K. The experimental loops are constructed based on the measured harmonics, and are plotted after subtracting a contribution expected from a frictional force proportional to velocity which would reproduce the zero amplitude limit of the observed damping, and removing the loop curvature induced by the k_2x^2 and k_2x^3 force terms. The experimental loops have a somewhat pointy character, but not nearly as pronounced as predicted by the stick-slip picture.

One would like to make the corresponding plots for the data at 4.2 K, where the r ratio is much closer to 4/3. Unfortunately, the performance of our instrument's photodiode array was degraded at that temperature, introducing a velocity-dependent time slewing of the transit zero crossing points. This did not significantly affect the measurements of oscillation frequency, amplitude, Q, and most of the harmonics, but did distort measurements of some of the harmonics making it impossible to extract a reliable hysteresis loop at 4.2 K.

Certainly our results are strongly suggestive of some kind of 'stick-slip' mechanism, although what the underlying physical basis for this might be is unclear. Returning to the question of what frequency dependence the observed nonlinear fiber damping component might introduce into the effective torsion constant in our planned G measurement, we note that both the apparent temperature independence of this component and the fact that the behavior is well represented by a frequency independent simple model together suggest that the nonlinear damping component should be frequency independent at a given amplitude, and hence not a source of bias in the G measurement.

5. Future plans

We have recently completed a much larger instrument, which will operate in a former Nike missile bunker in eastern Washington state where the microseismic background is much lower than in our Irvine lab. The new instrument will operate at 2 K, with much improved temperature control, and will use new photodiodes which should operate well at this temperature. We intend to extend our fiber studies to A15056, and possibly explore the effects of various treatments of a BeCu fiber.

Acknowledgements

We are indebted to Nadathur Krishnan for many contributions in the early days of this work, and to Arthur Nowick, Andrew Granato, and Terry Quinn for helpful discussions. This work was supported by NSF grant PHY-95 14944

References

[1] T.S. Ké, J. Alloys Comp. 122/212 (1994) 7.
[2] R.D. Newman, M.K. Bantel, Meas. Sci. Technol. 10 (1999) 445.
[3] K. Kuroda, Phys. Rev. Lett. 75 (1995) 2796.
[4] C.H. Bagley, G.G. Luther, Phys. Rev. Lett. 78 (1997) 3047.
[5] T.J. Quinn, C.C. Speake, L.M. Brown, Phil. Mag. A 65 (1992) 26.
[6] P.R. Saulson, Phys. Rev. D 42 (1990) 2437.
[7] A.S. Nowick, B.S. Berry, Anelastic Relaxation in Cystalline Solids, Academic, New York, Chapter 4, 1972.
[8] S. Matsumura, N. Kanda, T. Tomaru, H. Ishizuka, K. Kuroda, Phys. Lett. A 244 (1998) 4.
[9] Y.L. Huang, Ph.D. Thesis, Syracuse University, September 1996
[10] M.K. Bantel, Ph.D. Thesis, University of California at Irvine, 1998
[11] A.B. Lebedev, J. Phys. IV 6 (1996) C8–255.